



Improvements of mixing process in a rapidly tubular flame burner

Yoldoss Chouari¹, Wassim Kriaa¹, Hatem Mhiri¹, Philippe Bournot²

¹ UTTPI, National Engineering School of Monastir (ENIM), Av. Ibn El Jazzar, 5019 Monastir, Tunisia.

² IUSTI, UMRCNRS 6595, 5 rue Enrico Fermi, Technopôle de Château-Gombert, 13013 Marseille, France.

Received 12 July 2016; Received in revised form 5 Sep. 2016; Accepted 20 Sep. 2016; Available online 1 March 2017

Abstract

A three-dimensional simulation of a steady non-reactive mixing process in a rapidly mixed type tubular flame burner is carried out in order to examine the effects of the injectors' number ($N=2, 3, 4$ and 6), the swirl number ($Sw=0.46, 0.68, 1.05$ and 1.83) and the injector arrangements ($3-3$ and $4-2$). The mixing process is investigated by focusing on the following criterions: Particles trajectory, Central reverse zone (CRZ) and mixing layer thickness. The particles are tracked using a Lagrangian Discrete Phase Model (DPM). The numerical solutions are validated by comparing with previous experimental results. It is pertinent to note that the model predicts properly the flow field and the mixing in a rapidly tubular flame. The obtained results have generally shown, that for the same swirl number and same average axial velocity, the increase of injectors' number generates a larger reverse flow and decreases the mixing layer thickness. It is also shown that a high swirl number and same distribution of the injectors' number could significantly promote the mixing in rapidly tubular flame.

Copyright © 2017 International Energy and Environment Foundation - All rights reserved.

Keywords: Tubular flame burner; Mixing; Injectors' number, Mixing layer thickness; CFD; DPM.

1. Introduction

Swirling flows are commonly used where the mixture is desired, and are frequently encountered in several industrial applications such as exchangers [1-2], cyclone separators [3-5] and especially in various types of burners [6-9]. In this context, Syred and Beer [9] studied the flow structure and the mixing in different swirling burners configurations. It was shown that improving reactants mixing has a great influence on the combustion performance.

The Rapidly Tubular Flame Burner (RTFB) is a safe concept proposed by Ishizuka et al. [10]. In this burner, the reactants are separately introduced tangentially. Under the effect of centrifugal force, they mix quickly and after ignition the combustion rapidly mixed type tubular flame can be established. Several experimental studies of this type of burner have been provided [11-14]. That of Shi et al. [11-13] has discussed the mixing process, the flame structure, the extinction limits and the stability under different oxygen mole fractions. It was shown that the mixing layer thickness (δ) is inversely proportional to the square root of the injection velocity. This thickness (δ) has allowed to deduce the mixing time (τ_m) and to calculate the Damköhler number ($Da = \tau_m / \tau_r$ with τ_r is the reaction time). The Damköhler number has proved to be able to give a useful indication for the success or failure of the rapid

combustion in the RTFB [11, 12]. The authors have also studied the effect of swirl number and flow rate on mixing in a RTFB by varying the injectors' length. It was found that in order to improve mixing in this type of burner with four injectors, high Reynolds and swirl numbers are recommended. It should be noted that Shi et al. [11-14] examined experimentally the mixture effectiveness by varying only the width and the length of the injectors.

It is essential to have a general idea on the success/failure of the flame before the combustion test. However, the experimental studies are often limited by the bounds of cost and measurement techniques. To overcome these limits, various numerical simulations of the mixing in different burner configurations [15-19] have been proposed. By using the mixture fraction, Tatsumi et al. [16] have investigated the buoyancy and the swirl effects on mixing process in the miniature confined multijet. It was observed that, when the swirl is applied, the degree of asymmetry in multi-jet is reduced. Ranga Dinesh et al. [17] have studied the swirl effects on the mixing in a co annular swirl combustor. By analyzing respectively coherent structures, vortex breakdown bubbles and mean passive scalar distribution, Pathak et al. [19] have examined the effects of the streamline curvature on the mixing layer.

Most of these studies have only explored the mixing efficiency, in different burner configurations, by focusing on the mass fraction species [15, 16] or the coherent structures and vortex breakdown bubbles in the flow [17, 18]. This fact supports the present numerical study that provides a detailed investigation of the Rapidly mixed type Tubular Flame Burners (RTFB).

Hence, in order to improve the design of the RTFB a better understanding of the injectors' number influence on mixing process is mandatory. In what follows, the model validation and the numerical methods conducted in order to study the mixture effectiveness in a RTFB are first introduced. Then, the effects of the injectors' number, the swirl number and the injector arrangements on mixing process are discussed.

2. Burner configuration

The dimensions of the tubular flame burner used in the present study (Figure 1) correspond to those used in the experiments of Shi et al [13]. The inner diameter of the burner is $D_e=16\text{mm}$ and the total length is $L^*=160\text{mm}$. The burner has four rectangular tangential slits which are width $W=2\text{mm}$ and length L .

Due to the symmetry of the tubular burner geometry, only half the domain is modeled to decrease the grid number and thus to reduce the computational time.

Swirling flows are characterized by the dimensionless parameter called swirl number S . This number can be expressed as a function of input parameters - output of the burner, as follows: [9, 20-22].

$$S_w = \frac{\pi D_0 D_e}{4NLW} \quad (1)$$

where D_e is the outlet diameter, D_0 is the diameter of the main section of the burner.

To analyze the mixing process, the method adopted by Shi et al. [11-13] based on the injection of Magnesium oxide particles (MgO) was used (Figure 1). For the burner with four slits as shown in Figure 1, the Magnesium oxide particles (MgO) were injected with air into the horizontal slits (A), for the other two slits (B) non seeded airflow was injected.

Any design parameters of the slit will influence both the flow characteristics and mixing performance. Thus, we propose to study the effect of the injectors' number.

3. Grid system

The computational domains of different configurations were first generated and meshed by Gambit. A hexahedral mesh with a structured boundary layer mesh near the wall of the burner was used since it is much more computationally-efficient than the tetrahedral mesh. Typically, a hexahedral mesh requires half the resolution in each of the three directions' reduction for almost an order of magnitude in the number of elements. To reduce the total cell number and to avoid a very large difference in cell volume between adjacent cells, the axial mesh distribution is increased progressively from the downstream slits to the outlet region.

In order to assure the independence of the solution from the grid size, several computational trials with 431,472 cells to 1,083,704 cells were performed. By comparing the radial distribution of circumferential velocities, it was noted that the numerical results predicted by the grids 879,040 to 1,083,704 cells are similar.

Considering the computational effort, the selected grid (879,040 cells) is locally refined in the near injection slits and boundary walls ($\Delta y = \Delta z = 3.10^{-4}$) as well as near the burner axis ($\Delta y = \Delta z = 10^{-4}$) so as to predict more accurately the trajectory of particles and mixing process. Figure 2 shows the overall grid structures adopted in this research.

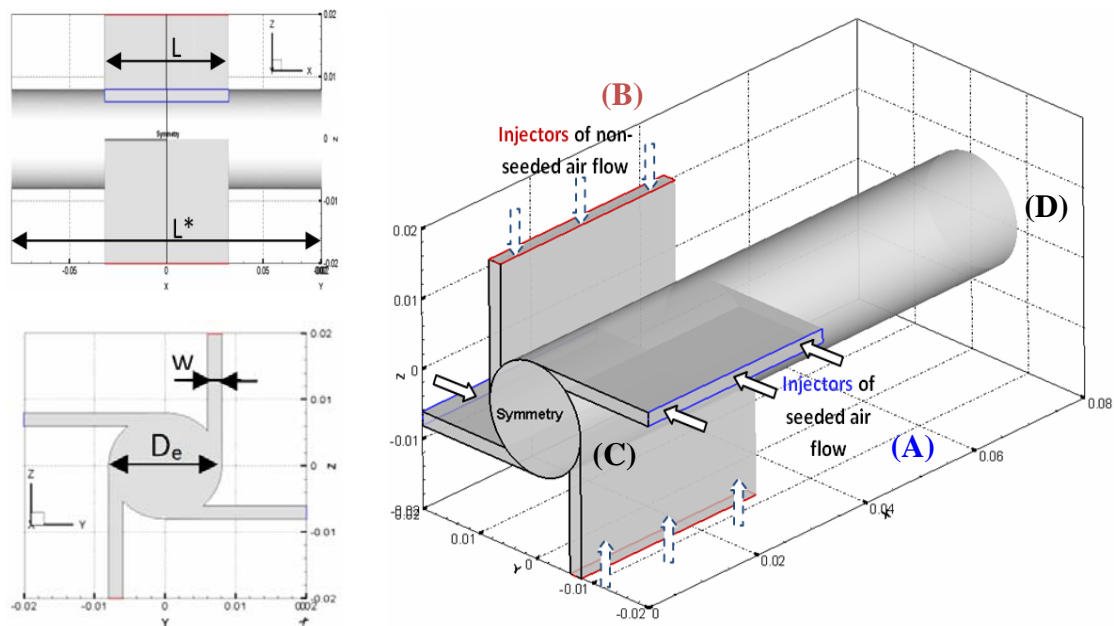


Figure 1. Schematic of the rapidly mixed type tubular flame burner.

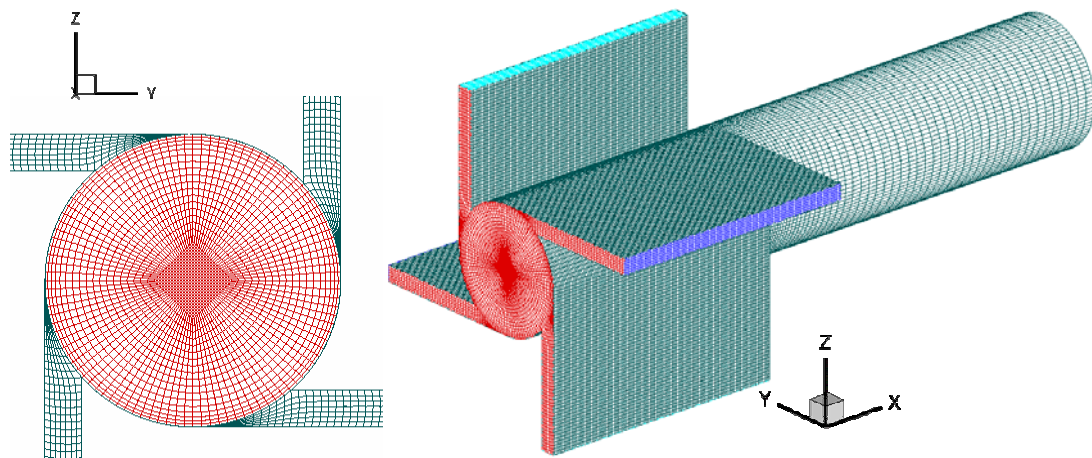


Figure 2. Grid system used in the computation.

4. Mathematical model

Solid particles motion in a flow field was described by the Eulerian–Lagrangian approach with a discrete phase method (DPM), i.e., the gas phase was treated as a continuum by solving Navier Stokes equations and the solid phase was calculated by tracking particles in the Flow field.

The considered fluid (air) is incompressible and the studied flow is steady. The particle phase is sufficiently dilute that particle-particle interactions and the effects of the particle volume fraction on the gas phase are negligible. In fact, the volume fraction of discrete phase is less than 10-12% [23]. The solid particles are spherical and non-deformable with a same diameter $d_p = 10^{-6}m$ and density

$\rho_p = 3580kg/m^3$. Since the particle density is considerably larger than that of the fluid, i.e., $\frac{\rho_p}{\rho_g} \gg 1$,

the buoyancy force, the Basset force, the pressure gradient force and the virtual mass force, could be neglected [24, 25].

The governing equations can be written as follows:

$$\frac{\partial}{\partial x_i}(\rho U_i) = 0 \quad (2)$$

$$\frac{\partial}{\partial x_j}(\rho U_i U_j) = -\frac{\partial P}{\partial x_i} + \frac{\partial}{\partial x_j}(\mu \frac{\partial U_i}{\partial x_j}) \quad (3)$$

To determine the trajectory of the solid particles, we integrate the force balance on particles [26]. The particles motions are so calculated with the following equation:

$$\frac{dU_p}{dt} = F_D (U - U_p) + g \left(\frac{\rho_p - \rho}{\rho} \right) \quad (4)$$

F_D is the drag force per unit of mass and velocity difference ($U - U_p$). U is the fluid phase velocity and U_p is the particle velocity. The Drag force is given by:

$$F_D = \frac{18\mu C_D Re_p}{\rho_p d_p^2} \frac{Re_p}{24} \quad (5)$$

μ is the molecular viscosity of the fluid, ρ is the fluid density, ρ_p is the density of particle, d_p is the particle diameter, Re_p is the relative Reynolds number and C_D is the drag coefficient given by:

$$C_D = a_1 + \frac{a_2}{Re_p} + \frac{a_3}{Re_p^2} \quad (6)$$

Where the a 's are constants that apply for smooth spherical particles over several ranges of Re_p given by [27].

5. Boundary condition and Solution strategies

Proper boundary conditions (Figure 1 and Table 1) have to be defined in order to solve the equations (1)-(6).

Numerical computations were carried out using Fluent 6.3 which is based on the finite volume method. The discretized equations, along with the initial and boundary conditions, were solved using the segregated solution method. In order to improve accuracy, the second order upwind scheme was applied. The SIMPLE method was used to calculate the pressure-velocity coupling. It uses a relationship between velocity and pressure corrections to enforce mass conservation and obtain the pressure field. The maximum residual of all variables was 10^{-4} in the converged solution.

Table 1. Boundary conditions.

Designation	Conditions	Values
Injectors of seeded air flow (N_1), (A)	Velocity inlet	$V_{inj} = V_{inj,F}$, 0.1-1 m/s
Injectors of non-seeded air flow (N_2), (B)	Velocity inlet	$V_{inj} = V_{inj,O}$, 0.1-1 m/s
Walls	No Slip	-
Symmetry (C)	Symmetry	-
Outlet (D)	Outflow	-

N_1 is the number of slits type A which inject air/MgO and N_2 is the number of slits type B which inject air.

6. Results and discussion

The objective of this work is to use CFD to model fluid flow and mixing process in a rapidly mixed type tubular flame burner. The aim is to discuss the effects of the injectors' number, the swirl number, the

inlet flow rate distribution on the particles trajectory, the central reverse zone and the mixing layer thickness.

For the verification of the model, the simulated results are compared with the experimental data of Shi et al. [13].

6.1 Validation of the numerical model

The validation of the numerical model is performed by confronting the calculated mixing layer thickness, Central Recirculation Zone (CRZ) diameter and circumferential velocities results to the experimental data of Shi et al. [13].

Figure 3 shows predicted and experimental values of the tangential velocity at the injectors' outlet for two burners ($S_w = 0.34$ and $S_w = 1.37$). The statistical accuracy of the proposed model is obtained by calculating the determination coefficient and the P-value for the two burners (Table 2). As it can be seen on Figure 3, the results are statistically significant with a high R-square (close to 1) and a low P-value (less than 10^{-7}). The agreement between the results is satisfactory which means that the adopted model describes statistically well the tangential velocity distributions for both burners.

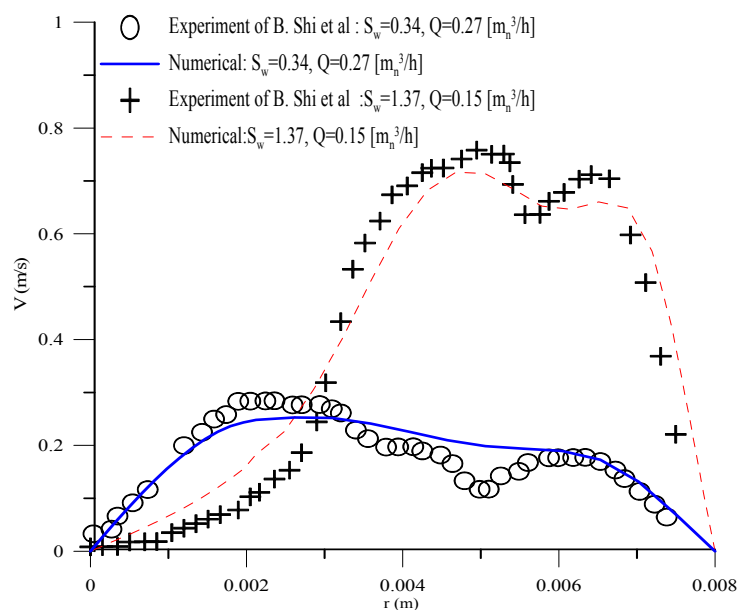


Figure 3. Predicted and experimental results of circumferential velocities for two burners.

Table 2. Summary of R-square and P-value.

	$S_w=0.34$	$S_w=1.37$
R-square	0.908	0.985
P-Value	10^{-7}	10^{-8}

The MgO particles are tangentially injected with air into the burner from the two horizontal slits of upper left and lower right. Whereas, only air was injected from the other slits. The flow structure is visualized by tracking the particles trajectory delimiting the flow injected through the horizontal slits.

Figure 4 shows a comparison between the predicted results (flow structure, mixing layer thickness, diameter of the central recirculation zone (CRZ)) and those obtained experimentally by Shi et al. [13]. It is clearly seen that the predicted flow structure is similar to that found by Shi et al. [13]. In fact, this method enables us to predict expansion and shrinkage of jet thickness after been ejected outside the slit. Moreover, at the same flow rate, ($Q_{\text{total air}} = Q_{\text{total seeded air}} = 0.15 \text{ m}^3/\text{h}$), the air injected from the low side gradually shrinks in width as the swirl number increases (case 1 and case 4).

The mixing layer thickness around the exit of the slit was determined after 45 degrees from the starting point which is defined as the inner edge of the lower right slit. The central recirculation zone is observed when the swirl number is superior to 0.6. It may be also noted that, for $S_w=0.69$, the CRZ diameter

gradually increases with an increase of the flow rate (case 2 and case 3). These findings have been also reported by Shi et al. [13].

Predicted and experimental mixing layer thickness and CRZ diameter are given in Table 3. For all the cases, the discrepancy between the results is less than 5%. Thus, the obtained results agree well with those of Shi et al. [13].

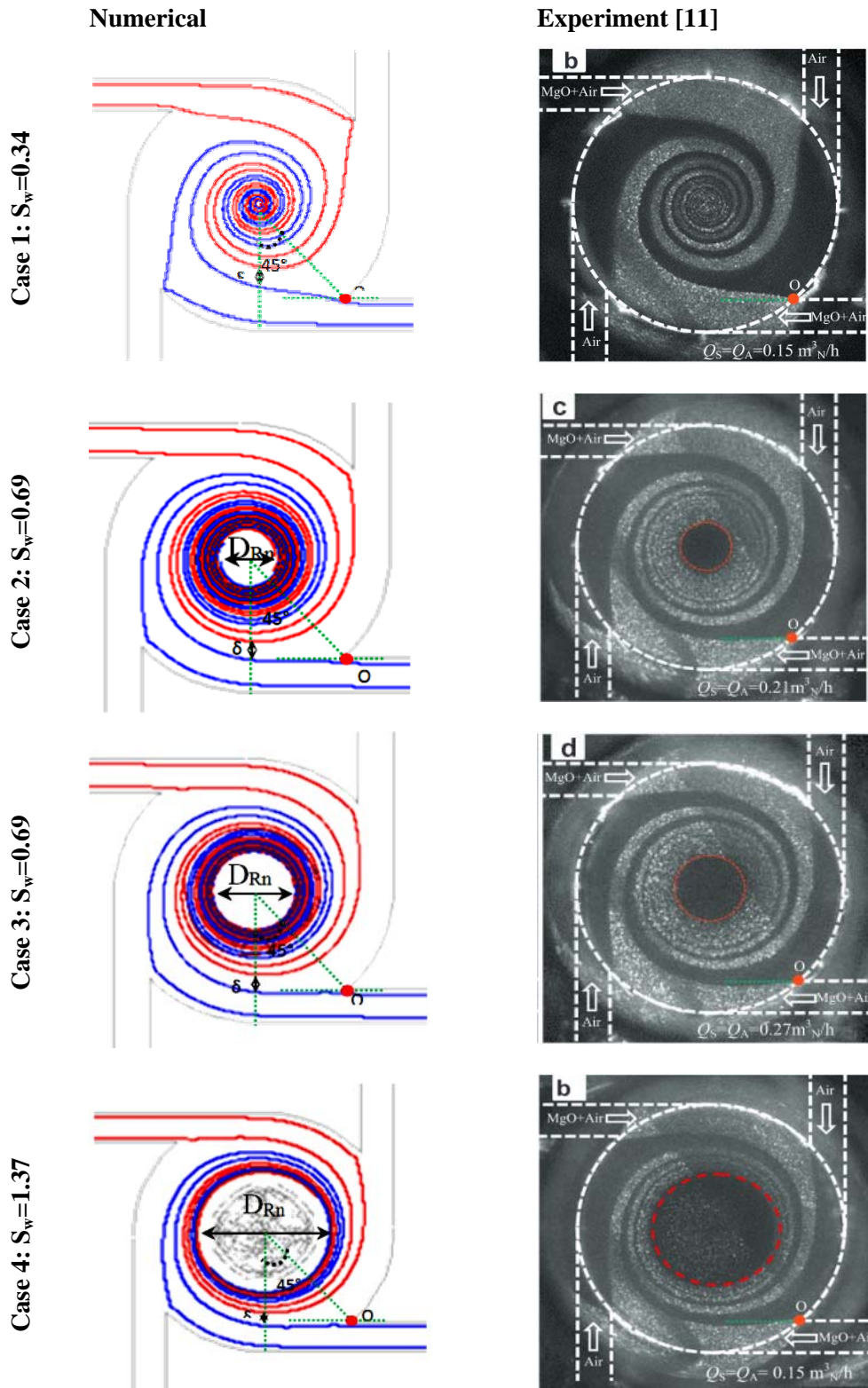


Figure 4. Predicted and experimental particles trajectories.

Table 3. Predicted and experimental mixing layer thickness and CRZ diameter.

	Case 1		Case 2		Case 3		Case 4	
	EXP	NUM	EXP	NUM	EXP	NUM	EXP	NUM
δ (mm)	1	1.05	0.95	1	0.94	0.96	0.75	0.79
D_R (mm)	0	0	3.1	3.2	4.32	4.45	8.51	8.59

6.2 Injectors' number effect

In what follows, the effects of the injectors' number on the mixing performance are discussed. Four cases with different number of injectors ($N=2, 3, 4, 6$) have been investigated (Table 4). The total flow rate is fixed at values equal to $32 \times 10^{-6} \text{ Kg s}^{-1}$, i.e. almost same mean axial velocity. It should be noted that for all the tested cases, the flow rate injected into each slit is equal to the total flow rate divided by the slit number.

Table 4. Specifications of burner design.

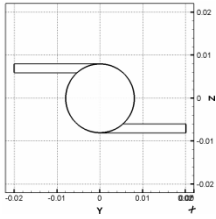
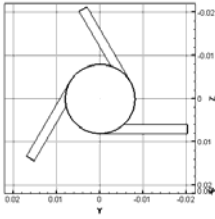
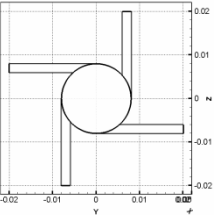
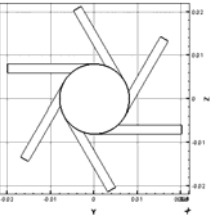
	Case 1	Case 2	Case 3	Case 4
Configurations				
Slit number	2	3	4	6
Slit length	24	16	12	8
Swirl number	1.83			

Figure 5 shows the particles trajectory in the cross section perpendicular to the tube axis varying with slit number. As it can be seen, the flow width shrinks after been ejected outside the slit creating a very intense centrifugal force. The dashed zone indicates surface contour of negative axial velocity which is used to identify the existence of the central reverse zone (CRZ). This zone eventually appears for all studied cases as the used swirl number is larger than the critical swirl number ($S_w > 0.6$).

Moreover, it is noted that the flow rate injected into each slit in case 4 is smaller than that injected into each slit in case 1. Consequently, the seeded air width after injection is decreased with an increase of injectors' number. On the other hand, the diameter of CRZ increases with an increase of injectors' number.

These observations lead to conclude that for the same swirl number and same average axial velocity, the increase of injectors' number promotes the mixing process in rapidly tubular flame.

Figure 6 shows the iso-surfaces indicating zero axial velocity ($U=0$) zones and the surface contour of negative axial velocity, on the plane, $OZ = 0 \text{ m}$. A central recirculation zone (CRZ), known as the vortex breakdown, is formed in the central region. The CRZ has the same conical form in all studied cases. This should be due to the decrease of the swirl motion while going downstream of the swirl generating device [28-30]. In fact, the decrease in centrifugal force reduces the diameter of CRZ while going away from slots. Additionally, the size of CRZ area becomes more extended due to the increase of the injectors' number. This confirms that the mixing process is more efficient in the case 4.

To quantify the effect of injectors' number on the mixing process, the mixing layer thickness is also analyzed. By varying the flow rates for all cases, the corresponding width δ is plotted as a function of $\frac{1}{\sqrt{V_t}}$ (see Figure 7). It is shown that the flow around the exit of the injector is dominated by a boundary

layer type flow [11-13]. It is also seen that at a constant total flow rate (Q_{total}) shown by the dotted line, the width δ gradually decreases with increasing injectors' number.

For fixed injection velocity, $V_t=0.33 \text{ m/s}$, and low injectors' number ($N=2$) (corresponding to the smaller values of total flow rate, $Q_{\text{total}}=N \cdot Q_{\text{inj}}$), the mixing layer thickness reaches its maximum. The case 1 ($N=2$) gives the upper limit of mixing coefficient ($K=6.3 \times 10^{-4} \text{ m}^{1.5} \text{ s}^{-0.5}$); by gradually increasing

the injectors' number, the total flow rate increases resulting the decrease of the mixing coefficient. These observations may conclude that the burner with high injectors' number assures a better mixing.

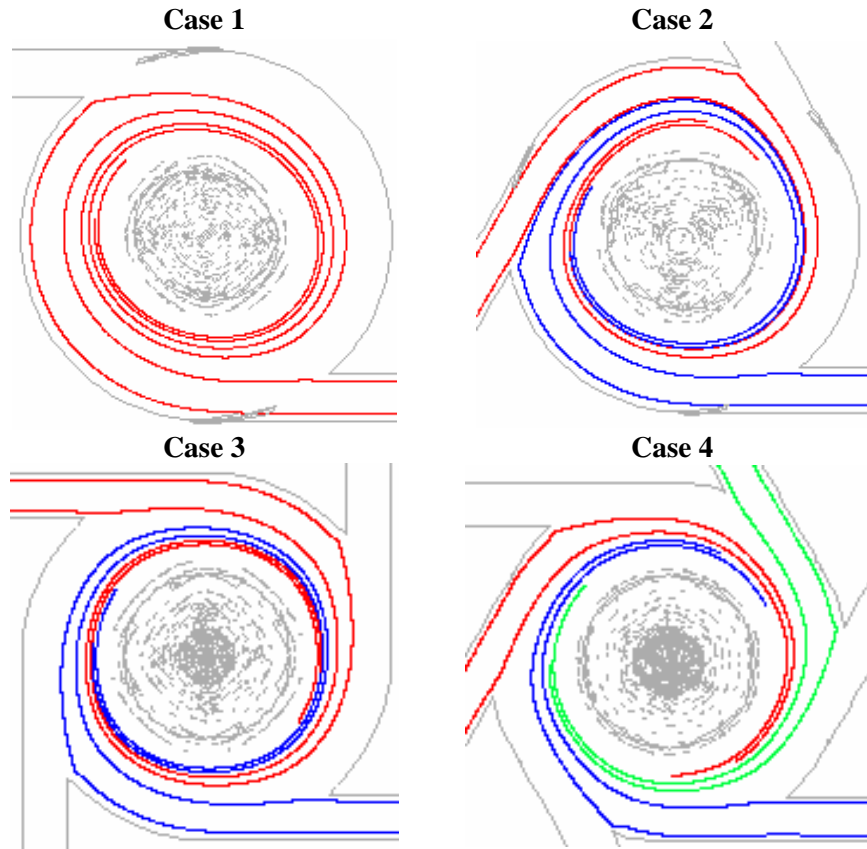


Figure 5. Particles trajectory in a cross section varying with injectors' number.

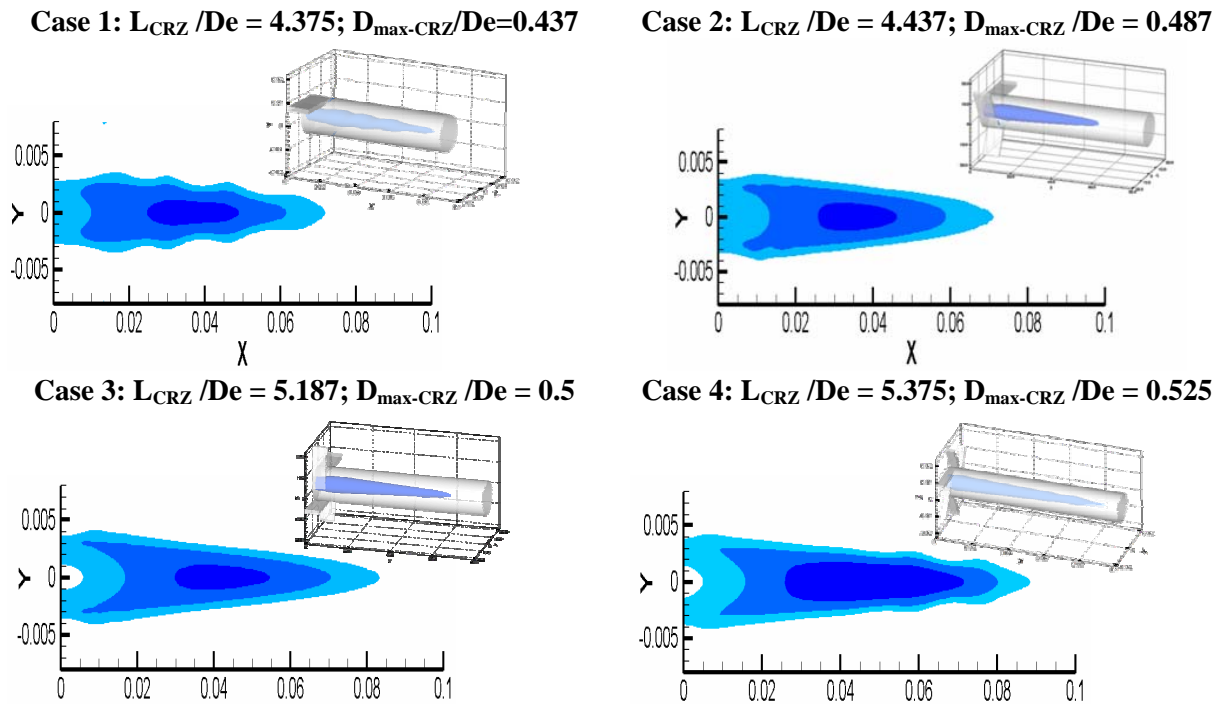


Figure 6. Central Reverse Zone (CRZ) for different cases.

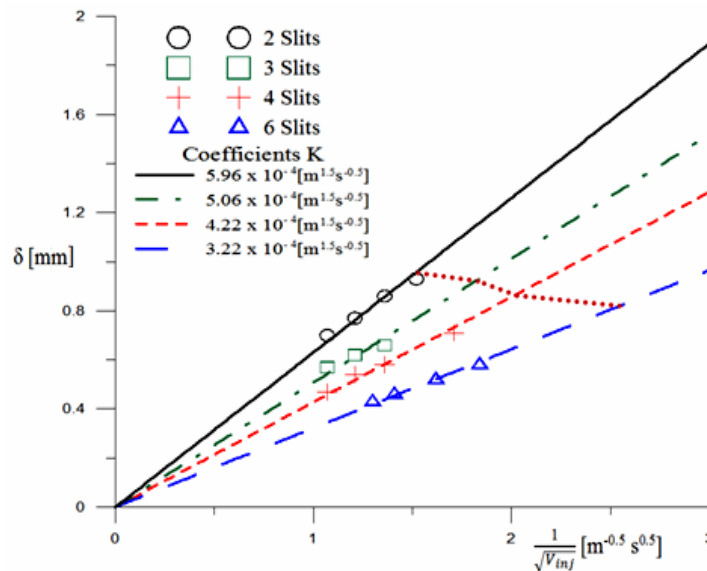


Figure 7. Boundary layer type flow around the exit of slit varying with the slits number.

6.3 Swirl number effect

Herein, the swirl number effect on the mixing performance is discussed for the configuration of high injectors' number ($N=6$). The total flow rate is fixed at about $48 \times 10^{-6} \text{ Kg s}^{-1}$. To analyze variable swirl intensity, four configurations of different injector lengths are considered. The computational configurations are summarized in Table 5. For all the tested cases, the flow rate injected into each slit is equal to the total flow rate divided by the slit number.

Table 5. Studied configurations.

	Case 1	Case 2	Case 3	Case 4
Slit Length (L)	32	22	14	8
Swirl number (S_w)	0.46	0.67	1.05	1.83

Figure 8 illustrates the particles trajectory in the cross section of different cases. For all studied cases, the particle trajectory allows to underline strongly helicoidally nature of flow.

In case 1 ($S_w=0.46$), the flow width expands after injection from the slit. In the central region of the configuration, the thickness between the particle trajectories becomes very small which means a good mixture between air + MgO and air. When the swirl number increases, as shown in case 4, the width of air flow shrinks after been ejected.

A central recirculation zone (CRZ) is observed in the center of burner in cases 2, 3 and 4. The CRZ diameter increases due to the increasing swirl number as a result of high centrifugal force.

The iso-surfaces indicating zero axial velocity ($U=0$) zones known as the central reverse zone are depicted in Figure 9. As seen previously, by increasing the swirl number to $S_w=0.67$ (case 2), a CRZ appears in the central region of the configuration. The CRZ has a conical form, its diameter decreases gradually in downstream of the injectors due to the decrease of the local swirl number. It is also noted that the CRZ increases in length with the increasing of swirl number.

Under various total flow rates, the width δ has been determined and the results for all tested cases are plotted as a function of $\frac{1}{\sqrt{V_t}}$ (see Figure 10). As would have been expected, the coefficient K decreases

with the increasing of swirl number. This has been confirmed for the case 1 ($S_w=0.46$) which has the higher coefficient $K=4.35 \times 10^{-4} \text{ m}^{1.5} \text{ s}^{-0.5}$ and for the case 4 ($S_w=1.83$) corresponding to the lower coefficient $K=3.22 \times 10^{-4} \text{ m}^{1.5} \text{ s}^{-0.5}$.

On the other hand, in case 2 ($S_w=0.67$) and case 3 ($S_w=1.05$), the coefficient K has the same value ($K=4 \times 10^{-4} \text{ m}^{1.5} \text{ s}^{-0.5}$). Additionally, at a constant flow rate, the average velocity of injection in case 2 is less important than that in case 3. These findings indicate that the mixing process is more efficient in case 3.

These coefficient values are a necessary database for further experimental work. In fact, these results give a general idea on the flame stability in a burner tubular flame before experimental tests.

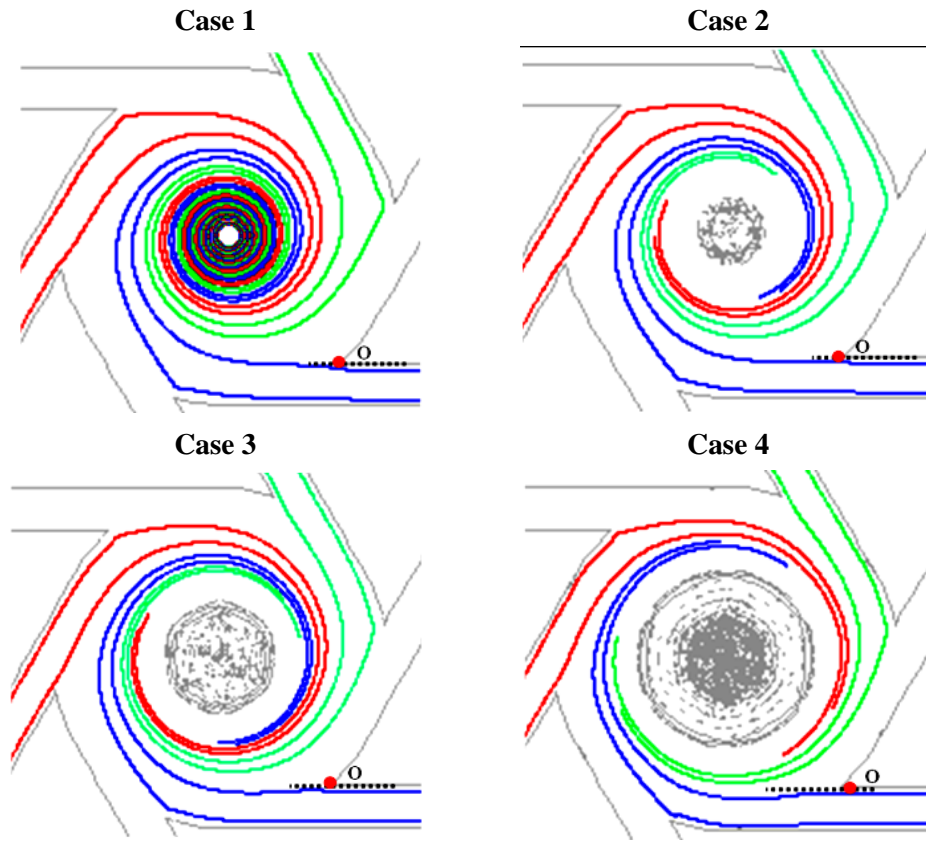


Figure 8. The particles trajectory in a cross section varying with the swirl number.

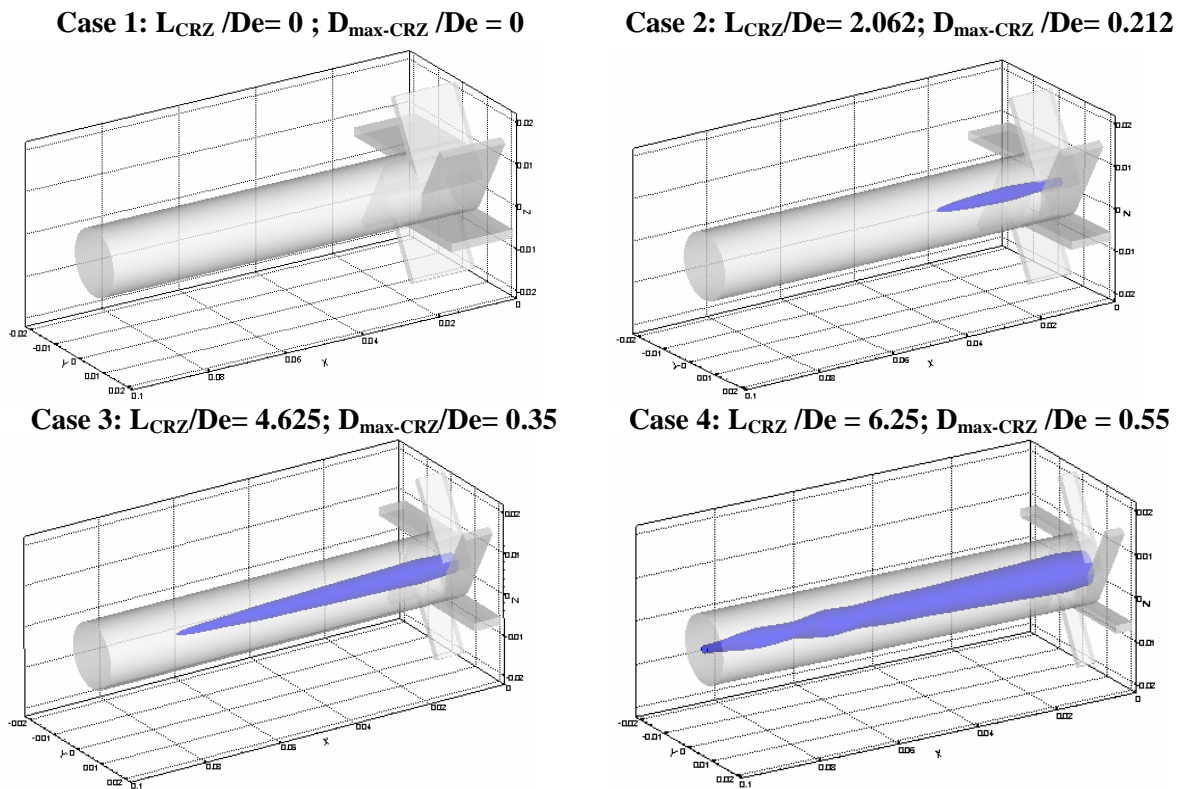


Figure 9. Iso-surface indicating zero axial velocity ($U=0$) zones for different cases.

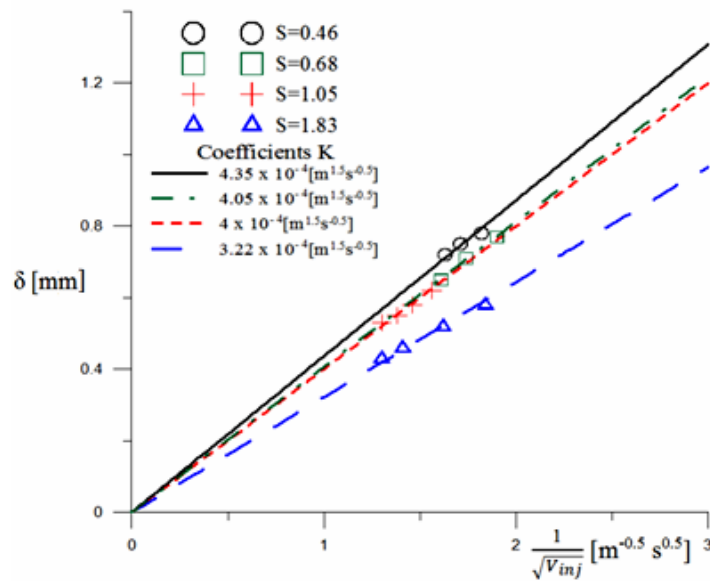


Figure 10. Boundary layer type flow around the exit of slit varying with the swirl number.

6.4 Effect of injectors' arrangement

The effect of injector arrangements on the mixing performance is now discussed. The total flow rate is fixed at about $17.2 \times 10^{-6} \text{ Kg s}^{-1}$ and ($Q_{\text{total seeded air}} = 0.5 Q_{\text{total air}}$). Table 6 presents the different investigated cases.

Table 6. Studied Configurations.

	Case 1	Case 2	Case 3	Case 4
N_1	3	4	3	4
N_2	3	2	3	2
$Q_a [10^{-6} \text{ Kg. s}^{-1}]$	3.82	2.865	3.82	2.865
$Q_s [10^{-6} \text{ Kg. s}^{-1}]$	1.91	2.865	1.91	2.865
Slit Length (L)	64	64	8	8
Swirl number (S_w)	0.23	0.23	1.83	1.83

Figure 11 shows the particles trajectory in a cross section of different cases. If we compare the results of case 1 with those of case 2, it is easily seen that the flow width expands after injection and that only in case 2, although the swirl number is the same for both cases. This could be explained by the difference in the arrangement of injectors.

If we consider the cases 3 and 4 where the CRZ is generated, it is noted that the injectors' arrangement in case 3 ($N_1=N_2=3$) leads to more efficient mixing. In fact, the injected flow shrinks more in its width in case 3.

To better visualize the maximum diameter and length of the recirculation zone in cases 3 and 4, the iso-surfaces indicating zero axial velocity ($U=0$) zones are shown in Figure 12. The CRZ has almost the same length in both cases. This result reveals that the injectors' arrangement has a significant influence on mixing, only in the vicinity of the slits outlet.

To quantify the effect of injectors' arrangement on the mixing process, the mixing layer thickness as a function of $\frac{1}{\sqrt{V_t}}$ is shown in Figure 13. If we consider cases 1 and 2, at low total flow rates and swirl

number, the measured δ shows a small deviation from the straight-line function of coefficient K. According to Shi et al. [13], this deviation is the result of the expansion flow after ejection from the slit as well as the effects of mass diffusion. It is also noted from Figure 13, that the mixing coefficient K in cases 1 and 3 ($N_1=N_2=3$) is smaller than that of cases 2 and 4 ($N_1 \neq N_2$), which enable us to conclude that the injectors' arrangement ($N_1=N_2=3$) leads to more efficient mixing process.

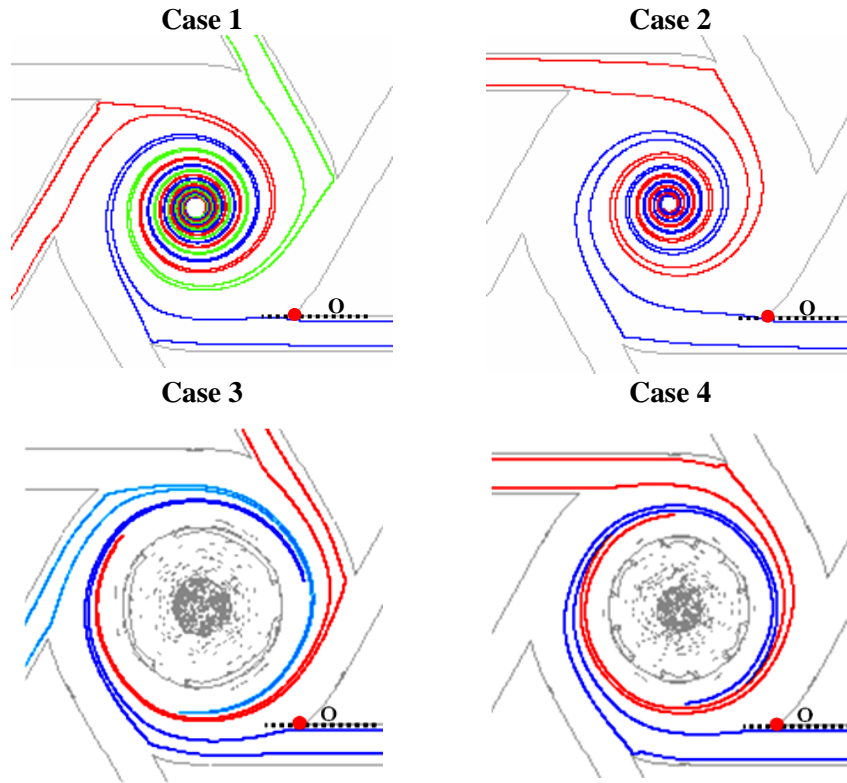


Figure 11. Trajectories of particles in a cross section varying with the N_1 and N_2 number.

Case 3: $L_{CRZ}/De = 2.425$; $D_{max-CRZ}/De = 0.45$

Case 4: $L_{CRZ}/De = 2.425$; $D_{max-CRZ}/De = 0.487$

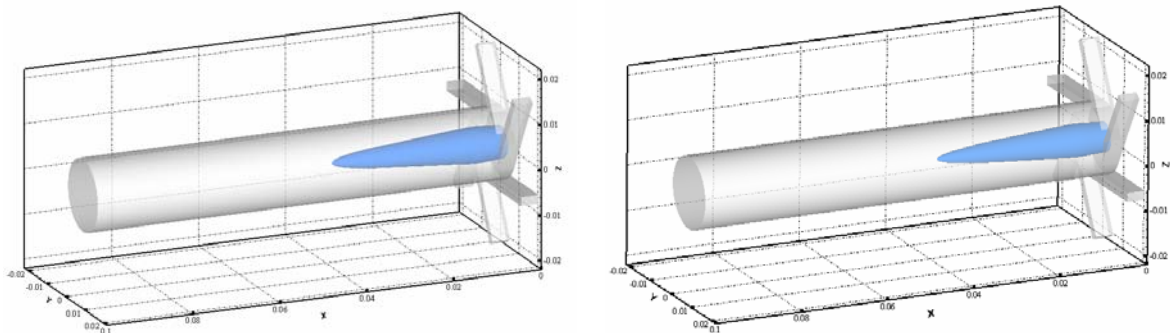


Figure 12. Iso-surface indicating zero axial velocity ($U=0$) zones for case 3 and case 4.

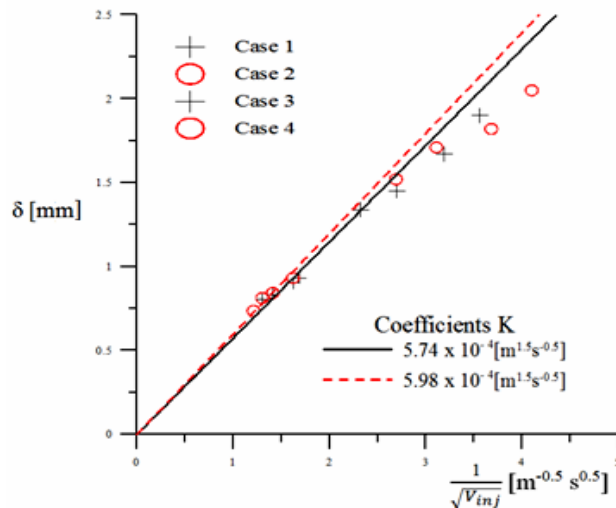


Figure 13. Boundary layer type flow around the exit of slit varying with the inlet flow rate distribution.

7. Conclusion

In this paper, a numerical investigation based on RANS method is performed to examine the effects of injectors' number, swirl number and injectors' arrangement on the mixing process in Rapidly mixed Type tubular Flame Burner (RTFB). The conclusions drawn from the present work are summarized in the following key notes:

- The agreement between the numerical results and the experimental data is satisfactory which means that the adopted model describes statistically well the mixing process in RTFB.
- For the same swirl number and same average axial velocity, the increase of injectors' number enhances the mixing process in rapidly tubular flame.
- High swirl number and same distribution of the injectors' number could significantly promote the mixing efficiency.

References

- [1] P. Eiamsa-ard, N. Piriyaarungroj, C. Thianpong, S. Eiamsa-ard, A case study on thermal performance assessment of a heat exchanger tube equipped with regularly-spaced twisted tapes as swirl generators, *Case Studies in Thermal Engineering*, 3, 2014, 86-102.
- [2] Christoph Biegger, Corrado Sotgiu, Bernhard Weigand, Numerical investigation of flow and heat transfer in a swirl tube, *International Journal of Thermal Sciences*, 96, 2015, 319-330.
- [3] Rainier Hreiz, Caroline Gentric, Noël Midoux, Numerical investigation of swirling flow in cylindrical cyclones, *chemical engineering research and design*, 89, 2011, 2521-2539.
- [4] Ons Tlili El May, Ines Mokni, Hatem Mhiri, Philippe Bournot, CFD investigation of a vortex tube: Effect of the cold end orifice in the temperature separation mechanism, *SATRESET*, 1, 2011, 84-89.
- [5] Rim Guizani, Inès Mokni, Hatem Mhiri, Philippe Bournot, CFD modeling and analysis of the fish-hook effect on the rotor separator's efficiency, *Powder Technology*, 264, 2014, 149-157.
- [6] Jeongseog Oh, Jeongjae Hwang, Youngbin Yoon, EINOx scaling in a non premixed turbulent hydrogen jet with swirled coaxial air, *international j. of hydrogen energy*, 35, 2010, 8715-8722.
- [7] C.Z. Xiouris, P. Koutmos, Fluid dynamics modeling of a stratified disk burner in swirl co-flow, *Applied Thermal Engineering*, 35, 2012, 60-70.
- [8] Nawel Khaldi, Yoldoss Chouari, Hatem Mhiri, Philippe Bournot, CFD investigation on the flow and combustion in a 300 MWe tangentially fired pulverized-coal furnace, *Heat and Mass Transfer*, DOI: 10.1007/s00231-015-1710-4.
- [9] N. Syred, J.M. Beér, Combustion in swirling flows: a review. *Combust. Flame*, 23, 1974, 143-201.
- [10] S. Ishizuka, T. Motodamari, D. Shimokuri, Rapidly mixed combustion in a tubular flame burner, *Proc. Combust. Inst.*, 31, 2007, 1085–1092.
- [11] B. Shi, D. Shimokuri, S. Ishizuka, Methane/oxygen combustion in a rapidly mixed type tubular flame burner, *Proc. Combust. Inst.*, 34, 2013, 3369–3377.
- [12] B. Shi, D. Shimokuri, S. Ishizuka, Reexamination on methane/oxygen combustion in a rapidly mixed type tubular flame burner, *Combust. Flame*, 161, 2014, 1310–1325.
- [13] B. Shi, J.Hu, H. Peng, S. Ishizuka, Flow visualization and mixing in a rapidly mixed type tubular flame burner, *Experimental Thermal and Fluid Science*, 54, 2014, 1-11.
- [14] B. Shi, J.Hu, S. Ishizuka, Carbon dioxide diluted methane/oxygen combustion in a rapidly mixed tubular flame burner, *Combust. Flame*, 162, 2014, 420-430.
- [15] E.S. Richardson, R. Sankaran, R.W. Grout, J.H. Chen, Numerical analysis of reaction–diffusion effects on species mixing rates in turbulent premixed methane–air combustion, *Combustion and Flame*, 157, 2010, 506–515.
- [16] Kazuya Tatsumi, Miyako Tanaka, Peter L. Woodfield, Kazuyoshi Nakabe, Swirl and buoyancy effects on mixing performance of baffle-plate-type miniature confined multijet, *International Journal of Heat and Fluid Flow*, 31, 2010, 45–56.
- [17] K.K.J. Ranga Dinesh, M.P. Kirkpatrick, K.W. Jenkins, Investigation of the influence of swirl on a confined coannular swirl jet, *Computers & Fluids*, 39, 2010, 756–767.
- [18] Y. Yang, Soren Knudsen Kaer, Large-eddy simulations of the non-reactive flow in the Sydney swirl burner, *International Journal of Heat and Fluid Flow*, 36, 2012, 47–57.
- [19] Manabendra Pathak, Anupam Dewan, Anoop K. Dass, An assessment of streamline curvature effects on the mixing region of a turbulent plane jet in crossflow, *Applied Mathematical Modelling*, 29, 2005, 711–725.

- [20] Chang, F., Dhir, V.K., Turbulent flow field in tangentially injected swirl flows in tubes. *International Journal of Heat and Fluid Flow*, 15, 1994, 346–356.
- [21] J.M. Beer, N.A. Chigier, T.W. Davies, K. Bassindale, Laminarization of turbulent flames in rotating environments, *Combust. Flame*, 16, 1971, 39–45.
- [22] A. Zawadzki, J. Jarosinski, Laminarization of flames in rotating flow, *Combust. Sci. Technol.*, 35, 1983, 1–13.
- [23] S. Elghobashi, On predicting particle-laden turbulent flows, *Appl. Sci. Res.*, 52, 1994, 309–329.
- [24] D.E. Stock, Particle dispersion in flowing gases, *Freeman Scholar Lecture, J. Fluids Eng.*, 118, 1996, 4–17.
- [25] Wenjing Sun, Wenqi Zhong, Yong Zhang S, LES-DPM simulation of turbulent gas-particle flow on opposed round jets, *Powder Technology*, 270, 2015, 302–311.
- [26] Fluent, FLUENT 6.3 user's guide, 2006.
- [27] S.A. Morsi, A.J. Alexander, An investigation of particle trajectories in two-phase flow systems, *J. Fluid Mech.*, 55, 1972, 193–208.
- [28] Osami Kitoh, Experimental study of turbulent swirling flow in a straight pipe, *Journal of Fluid Mechanics* 225, 1991, 445–479.
- [29] Rainier Hreiz, Caroline Gentric, Noël Midoux, Numerical investigation of swirling flow in cylindrical cyclones, *chemical engineering research and design*, 89, 2011, 2521–2539.
- [30] Mantilla, I., Bubble trajectory analysis in gas–liquid cylindrical cyclone separators. Master's thesis, The University of Tulsa. 1998.



Yoldoss Chouari is a Tunisian student in the National Engineering School of Monastir, in Tunisia. She is a member of the unit of heat transfer and thermodynamics of the industrial processes group. She received an engineering diploma in the field of energy and environment and a master's degree in the same field. Currently she is working on her Ph.D. degree.
E-mail address: yoldoss.chouari@yahoo.fr



Wassim Kriaa is an assistant professor of industrial engineering at the National Engineering School of Tunis. He received a Ph.D. degree of engineering in energy, in 2006 from Monastir University. His research contributions have been in the fields of industrial applications of jets and environmental problems. He has published 12 scientific articles.
E-mail address: kriaawas@yahoo.fr



Hatem Mhiri is a professor in the National Engineering School of Monastir, in Tunisia. He is a member of the unit of heat transfer and thermodynamics of the industrial processes group. He received a Ph.D. degree in the field of fluid mechanics and turbulence in 1986. He received in 1999 the H.D.R. degree, in energy, from Tunis University. His research is focused on industrial problems. He has published 104 scientific articles.
E-mail address: hatem.mhiri@enim.rnu.tn



Philippe Bournot is a professor of fluid mechanics at Aix-Marseilles University. He performs his research in the Laboratory IUSTI, in the “Risk Transfer” team, which he directed until 2009. A specialist in laser–matter interaction, he defended a thesis on the development of detonation waves maintained by CO₂ laser. He then worked in the field of industrial lasers and led European contracts on this topic. His current activities concern the application of fluid mechanics to natural risks in industrial and environmental problems.
E-mail address: philippebournot@yahoo.fr